

*Article*

## Photocatalytic Degradation of Phenol over Highly Visible-light Active BiOI/TiO<sub>2</sub> Nanocomposite Photocatalyst

Natkritta Boonprakob<sup>1,\*</sup>, Weerasak Chomkitichai<sup>1</sup>, Jiraporn Ketwaraporn<sup>1</sup>,  
Aimon Wanaek<sup>2</sup>, Burapat Inceesungvorn<sup>3</sup>, and Sukon Phanichphant<sup>4</sup>

<sup>1</sup> Department of Chemistry, Faculty of Science and Technology, Uttaradit Rajabhat University, Uttaradit 53000, Thailand

<sup>2</sup> Department of Physics, Faculty of Science and Technology, Uttaradit Rajabhat University, Uttaradit 53000, Thailand

<sup>3</sup> Department of Chemistry, Faculty of Science, Chiang Mai University, Chiang Mai 50200, Thailand

<sup>4</sup> Materials Science Research Center, Faculty of Science, Chiang Mai University, Chiang Mai 50200, Thailand

\*E-mail: nboonprakob@gmail.com

**Abstract.** BiOI/TiO<sub>2</sub> nanocomposites were successfully prepared by the two-step method, co-precipitation/solvothermal method. The amount of BiOI in the composites were varied as 0, 5.0, 7.5, 10.0 and 12.5 mol%. XRD results exhibited sharp and narrow diffraction peaks of both BiOI and TiO<sub>2</sub> in all composite samples. Morphologies of as-prepared samples consisted of spherical shapes of TiO<sub>2</sub> and nanosheets of BiOI. Diffuse Reflectance UV–visible (DR–UV–vis) spectra of composites drastically shifted into the visible range and the reduced band gap energies were observed. The composites obviously showed an enhanced phenol degradation of *ca.* 6 times higher than that of pure BiOI, pure TiO<sub>2</sub> and Degussa P25. The maximum photocatalytic activity of *ca.* 68% was found for 10.0 mol% BiOI/TiO<sub>2</sub> nanocomposite because of its increased visible light harvesting ability and its efficient electron–hole separation efficiency as observed from DR–UV–vis and photoluminescence spectra results.

**Keywords:** Bismuth oxyiodide, titanium dioxide, nanocomposites, phenol.

ENGINEERING JOURNAL Volume 21 Issue 1

Received 21 March 2016

Accepted 19 May 2016

Published 31 January 2017

Online at <http://www.engj.org/>

DOI:10.4186/ej.2017.21.1.81

## 1. Introduction

Phenol is an important toxic organic compound, which is the major source of water pollutant releasing from industrial as herbicide, pesticide, polymeric precursor and paint [1]. Regarding to the major chemical affected water pollution, the wastewater purification is becoming an important major investigation. The typical wastewater treatment including activated carbon or silica-alumina adsorption was used. Semiconductor photocatalytic technique has been utilizing for degradation or mineralization of aquatic phenolic compounds for several decades [2–4]. For this purpose, TiO<sub>2</sub> photocatalyst has been extensively investigated due to its properties such as high physical and chemical stability, non-toxicity and low cost [5]. However, the major limitation of TiO<sub>2</sub> is that it can only be activated under UV light. Therefore, many researchers have focused on an improvement of the light absorptivity of TiO<sub>2</sub> usually by forming a heterojunction with other visible-light-active materials, so that an effective utilization of solar light would be attained [6–8]. Moreover, the hybrid material also offers an efficient electron-hole transfer which benefits the separation of photoinduced charge carriers, hence enhancing the photocatalytic activity of the system [9]. Recently, BiOI has attracted a considerable attention due to its narrow band gap of 1.7–1.9 eV [10] which can largely harvest the visible light. Therefore, incorporating TiO<sub>2</sub> with BiOI may provide the material with better photocatalytic performance. Previous studies have shown that photocatalytic degradation of dyes over BiOI/TiO<sub>2</sub> composite is superior to those over TiO<sub>2</sub> and BiOI individually [11, 12]. The reverse microemulsions protocol for BiOI composite synthesis which mainly focuses on the use of surfactants was reported [13]. However, the amounts of BiOI used to composite with TiO<sub>2</sub> in those literatures are quite high (50–75 wt.%) and the synthesis method for the composite is rather complicated [14]. Therefore, an investigation on a facile synthesis method for the BiOI/TiO<sub>2</sub> heterostructure is mainly focused in this present work. The two-step co-precipitation/solvothermal method was successfully employed as the synthesis method of BiOI/TiO<sub>2</sub> composite. The photocatalytic efficiencies of prepared samples were also evaluated by phenol photodegradation under visible light irradiation.

## 2. Experimental

### 2.1. Nanocatalyst Preparation

Pure BiOI was prepared by co-precipitation method. Briefly, 1.092 g of Bi(NO<sub>3</sub>)<sub>3</sub>·5H<sub>2</sub>O was dissolved in 30 mL of absolute ethanol and stirred until the clear solution was obtained. An aqueous KI solution was then added into the above solution, keeping Bi:I in 1:1 mole ratio. The suspension pH was adjusted to 4.0 by NH<sub>4</sub>OH. Then, the reaction was aged at 80 °C for 5 h. The precipitate was washed and dried at 60 °C for 24 h. Pure TiO<sub>2</sub> was synthesized by modified sol-gel method similar to that reported previously [15]. BiOI/TiO<sub>2</sub> nanocomposites were prepared by the two-step co precipitation/low-temperature solvothermal method. Typically, 1.0 g of as-synthesized TiO<sub>2</sub> powder was sonicated for 1 h and then added carefully into the mixture of Bi(NO<sub>3</sub>)<sub>3</sub>·5H<sub>2</sub>O and KI. A 100 μL of ethylene glycol was subsequently dropped into the mixture. The mol percentages of BiOI were varied as 0, 5.0, 7.5, 10.0 and 12.5%, respectively. The suspension pH was adjusted to 4.0. The suspension was then subjected to solvothermal treatment at 100 °C for 5 h. After the treatment, the sample was washed by DI water for 3 times and dried at 60 °C for 24 h.

### 2.2. Sample Characterization

XRD pattern was characterized to confirm the crystalline phase of the prepared samples by X-ray diffractometer Rigaku MiniFlex II (Cu-K<sub>α</sub> radiation). BET N<sub>2</sub> adsorption for specific surface area determination at the temperature of liquid nitrogen was investigated by Autosorb-1MP-Quantachrome. Optical property of the photocatalysts was analyzed by DR-UV-vis Spectrophotometer (Shimazu, UV-3101PC) and photoluminescence spectroscopy (PL, Avantas-2048TEC). Morphology and microstructure of the as-prepared samples were examined by scanning electron microscope equipped with energy dispersive X-ray spectroscopy (SEM-EDS, JEOL JEM-2010) and transmission electron microscope (TEM, Philips TECHNAI 12).

### 2.3. Photocatalytic Activity Studies

The photocatalytic degradation of phenol was evaluated under visible light irradiation ( $\lambda > 400$  nm). For comparison, the photocatalytic degradation of phenol over Degussa P25 and direct photolysis were also investigated under the same conditions. The photocatalytic degradation of phenol was evaluated under visible light irradiation ( $\lambda > 400$  nm) using a 50 W of halogen lamp with an intensity of 640 W/m<sup>2</sup>. The initial concentration phenol solution was 10 mg/L. The suspension pH was adjusted to 8.0±0.30 by using 0.1 M NH<sub>4</sub>OH and HClO<sub>4</sub> solution. A 0.8 g/L of catalyst suspension was kept in the dark for 30 min to obtain adsorption/desorption equilibrium. After irradiation, 4 mL of suspension was withdrawn periodically in every 45 min and filtered by a Millipore filter (0.22 μm). Then, the phenol solution was dyed by the 4-aminoantipyrine colorimetric method (APHA, 1992) [16]. The maximum absorbance at 504 nm was analyzed using UV-vis spectrophotometer (PG Instruments, T90).

## 3. Results and Discussion

### 3.1. Crystal Phase and Microstructure Analysis

The XRD patterns of pure BiOI, pure TiO<sub>2</sub> and BiOI/TiO<sub>2</sub> nanocomposites are shown in Fig. 1. The peaks at 2θ of 9.6°, 19.5°, 29.6°, 31.6°, 37.0°, 39.3° and 45.3° correspond to (001), (002), (012), (110), (013), (014) and (112) crystal planes of tetragonal BiOI (JCPDS file No.10-0445). Sharp and narrow XRD peaks of pure BiOI indicate that the sample is well crystallized [17]. Pure TiO<sub>2</sub> calcined at 600 °C exhibits the characteristic peaks at 25.3°, 37.8°, 48.0°, 53.9°, 54.9° assignable to the (101), (004), (200), (105) and (211) crystal planes of anatase TiO<sub>2</sub> (JCPDS file No. 21-1272) [18]. The XRD spectra of BiOI/TiO<sub>2</sub> nanocomposites present the characteristic peaks of both TiO<sub>2</sub> and BiOI, indicating the composite nature of the prepared samples. As the BiOI content in BiOI/TiO<sub>2</sub> composite is increased, the relative peak intensity of BiOI also increases. By using the strongest peaks of anatase TiO<sub>2</sub> (101) and BiOI (012) planes, the average crystallite sizes of TiO<sub>2</sub> and BiOI, calculated according to the Scherrer's equation (Eq. (1)), can be obtained as presented in Table 1 [19].

$$L = 0.89\lambda/\beta(\cos \theta) \quad (1)$$

where  $\lambda$  is the wavelength of the X-ray in nanometer (0.154 nm),  $\beta$  is the width of the XRD peak at half peak-height (FWHM) in radian,  $\theta$  is the angle between the incident and diffracted beams in degree, and  $L$  is the average crystallite size of the sample in nm. Specific surface area ( $S_{\text{BET}}$ ) of all synthesized photocatalysts is also shown in Table 1. Upon increasing BiOI content, the  $S_{\text{BET}}$  of the composite significantly decreases due to the low surface area nature of BiOI. In our study, the lowest  $S_{\text{BET}}$  is found as 50.87 m<sup>2</sup>/g for 12.5 mol% BiOI/TiO<sub>2</sub> composite.

Table 1. Average crystallite size and specific surface area of photocatalysts.

Sample	Crystallite size (nm)		$S_{\text{BET}}$ (m <sup>2</sup> /g)
	anatase TiO <sub>2</sub> (101) plane	BiOI (012) plane	
Pure TiO <sub>2</sub>	25.02	-	110.24
5.00 mol% BiOI/TiO <sub>2</sub>	22.85	16.29	80.30
7.50 mol% BiOI/TiO <sub>2</sub>	22.43	16.31	74.14
10.0 mol% BiOI/TiO <sub>2</sub>	22.25	16.32	69.30
12.5 mol% BiOI/TiO <sub>2</sub>	22.20	16.34	50.87
Pure BiOI	-	23.16	7.50

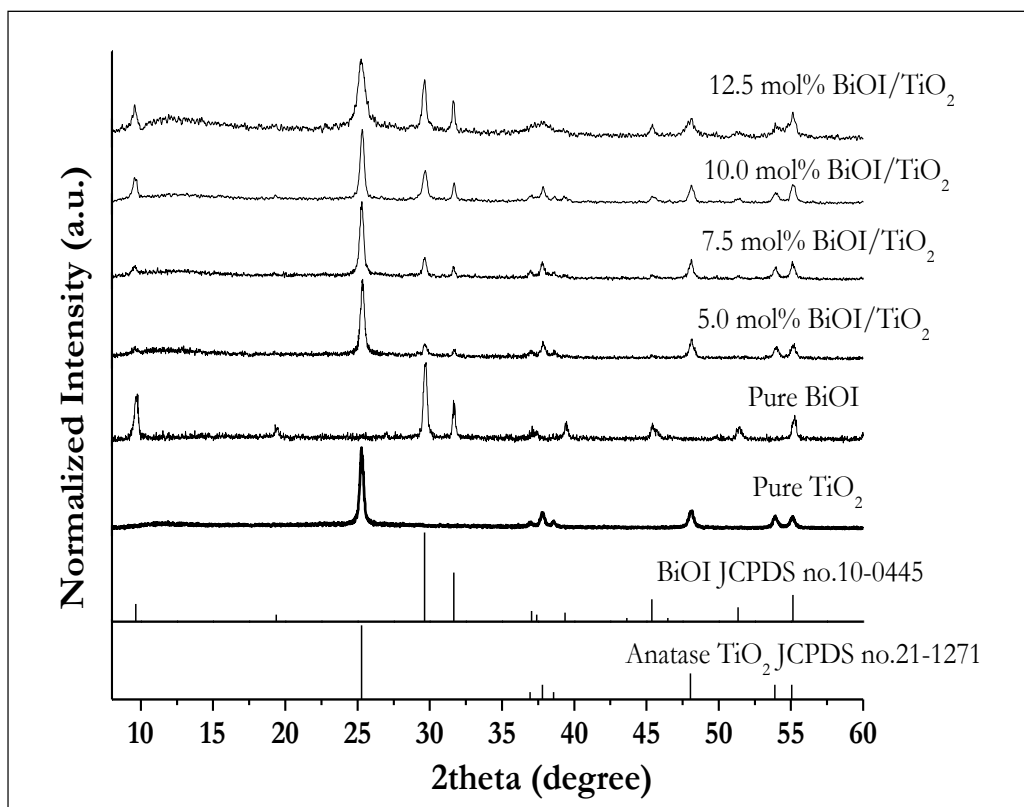


Fig. 1. XRD patterns of pure TiO<sub>2</sub>, pure BiOI and BiOI/TiO<sub>2</sub> nanocomposites.

Figure 2 shows the morphology and microstructure of pure TiO<sub>2</sub>, pure BiOI and 10.0 mol% BiOI/TiO<sub>2</sub> characterized by SEM-EDS. Pure TiO<sub>2</sub> (Fig. 2(a)) presents as aggregated spherical particles with different sizes in the range of 0.3–0.7 μm. Meanwhile, pure BiOI (Fig. 2(b)) appears as plate-like structure and agglomerations of plate building units. Figure 2(c) shows that BiOI plates are covered with several small TiO<sub>2</sub> particles. The EDS analysis of BiOI/TiO<sub>2</sub> nanocomposite (Fig. 2(d)) also confirms the presence of Ti, O, Bi and I in the composite catalyst.

TEM micrographs of TiO<sub>2</sub>, BiOI, and 10.0 mol% BiOI/TiO<sub>2</sub> nanocomposite are shown in Fig. 3. The morphology of pure TiO<sub>2</sub> (Fig. 3(a)) reveals almost spherical shape with the average particle size of 20–30 nm, which well relates to the crystallite size calculated by Scherrer equation. Figure 3(b) shows the aggregation of plate-like structure of BiOI with a diameter of *ca.* 50 nm. For 10.0 mol% BiOI/TiO<sub>2</sub> nanocomposite in Fig. 3(c), TiO<sub>2</sub> nanoparticles are found buried in BiOI sheets. Figure 3(d) also shows close interfacial contacts between TiO<sub>2</sub> nanoparticles and thin lamellar of BiOI in the composite which would lead to an efficient electron-hole transfer, and an enhanced photocatalytic activity as a consequence [19]. High resolution TEM micrograph showing lattice fringes of 10.0 mol% BiOI/TiO<sub>2</sub> in Fig. 3(d) reveals the crystalline nature of the particles. The lattice spacings of 0.34 nm and 0.28 nm follow the *d*-values of anatase TiO<sub>2</sub> (101) [20] and BiOI (110) planes [21], respectively.

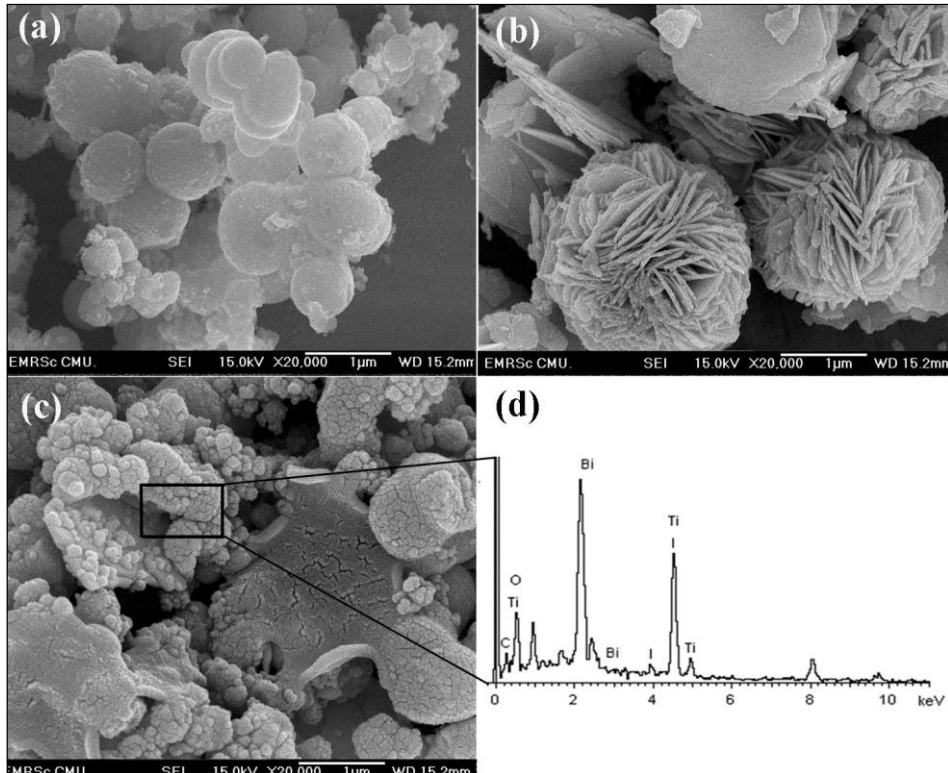


Fig. 2. FE-SEM images of (a) Pure  $\text{TiO}_2$ ; (b) Pure  $\text{BiOI}$ ; (c) 10.0 mol%  $\text{BiOI}/\text{TiO}_2$  composite and (d) the EDX spectrum of (c).

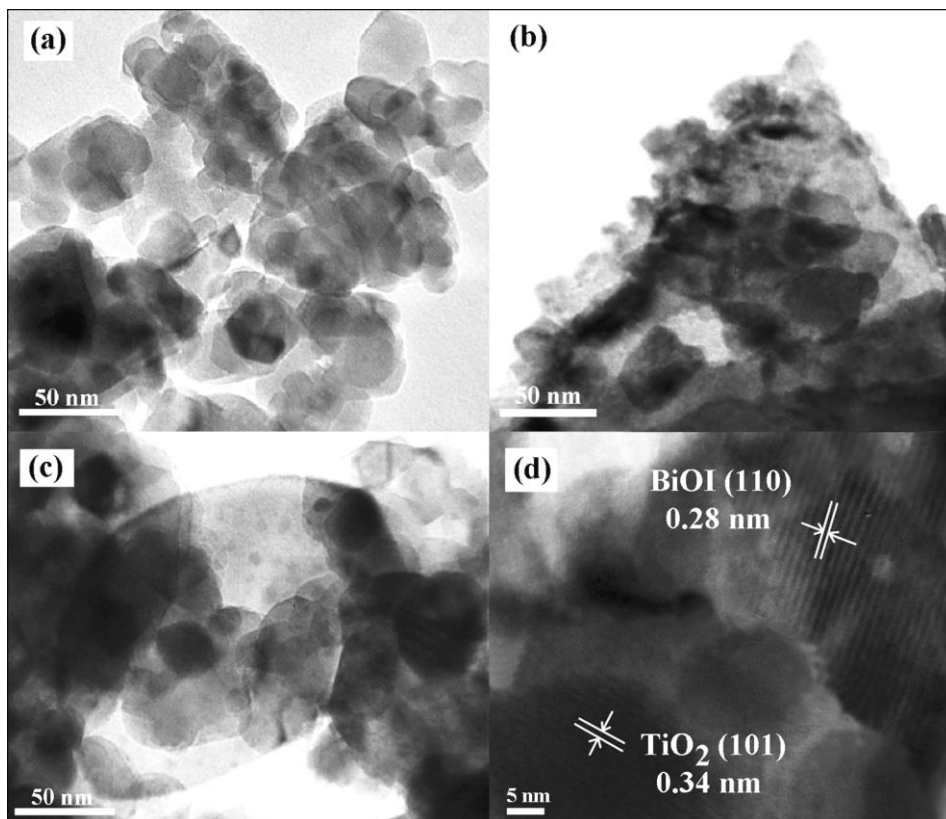


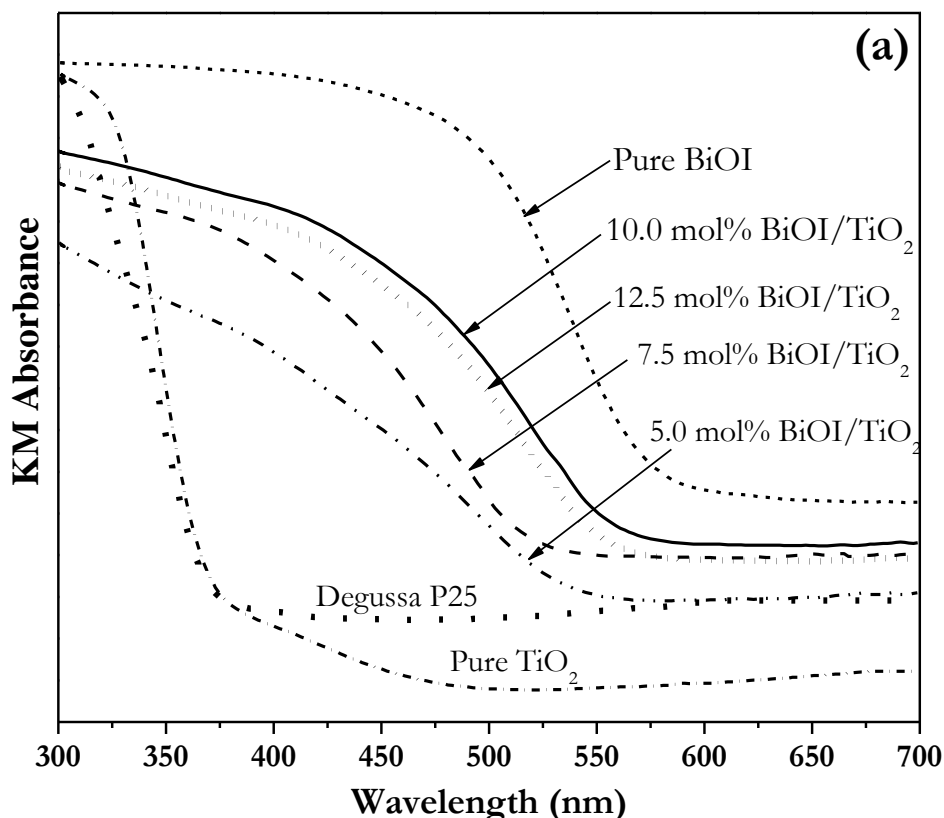
Fig. 3. TEM micrographs of (a) pure  $\text{TiO}_2$ , (b) pure  $\text{BiOI}$  and (c,d) 10.0 mol%  $\text{BiOI}/\text{TiO}_2$  nanocomposite.

### 3.2. UV–vis Diffuse Reflectance Spectra

The diffuse reflectance UV–vis spectra (DR–UV–vis) of pure BiOI, pure TiO<sub>2</sub>, Degussa P25 and BiOI/TiO<sub>2</sub> composite catalysts at different Bi/Ti molar ratios are presented in Fig. 4(a). From the figure, pure BiOI shows the strongest light absorbance with the absorption onset at *ca.* 630 nm, whereas pure TiO<sub>2</sub> and Degussa P25 present the absorption edges at *ca.* 385 and *ca.* 387 nm, respectively. A significant shift of TiO<sub>2</sub> absorption edge into the visible light region can be clearly observed upon incorporation TiO<sub>2</sub> with BiOI. According to Eq. (2), optical band gap energy ( $E_g$ ) of the catalysts can be obtained as illustrated in Fig. 4(b):

$$(\alpha h\nu)^{1/2} = A(h\nu - E_g) \quad (2)$$

where,  $h\nu$  is the photon energy,  $\alpha$  is the absorption coefficient,  $h$  is Planck's constant and  $\nu$  is light frequency [22]. From Fig. 4(b), the band gap energies of pure TiO<sub>2</sub>, pure BiOI, 5.0, 7.5, 10.0 and 12.5 mol% BiOI/TiO<sub>2</sub> composites are approximately 3.22, 1.86, 2.16, 2.20, 2.04 and 2.08 eV, respectively. The lowest band gap energy of composite photocatalyst is received from 10.0 mol% BiOI/TiO<sub>2</sub> (2.04 eV). The significant red-shift of the light absorption range upon increasing BiOI amount in the composite sample corresponds well with the reduced band gap energy. This suggests the high efficiency of visible-light utilization of the BiOI/TiO<sub>2</sub> composite which would lead to high generation of electron-hole pairs and probably an enhanced photocatalytic activity [23]. It is clear from our finding that by forming BiOI/TiO<sub>2</sub> composite, optical and physical properties of the materials change significantly. This also affects the phenol photodegradation activity of the materials as shown in the next section.



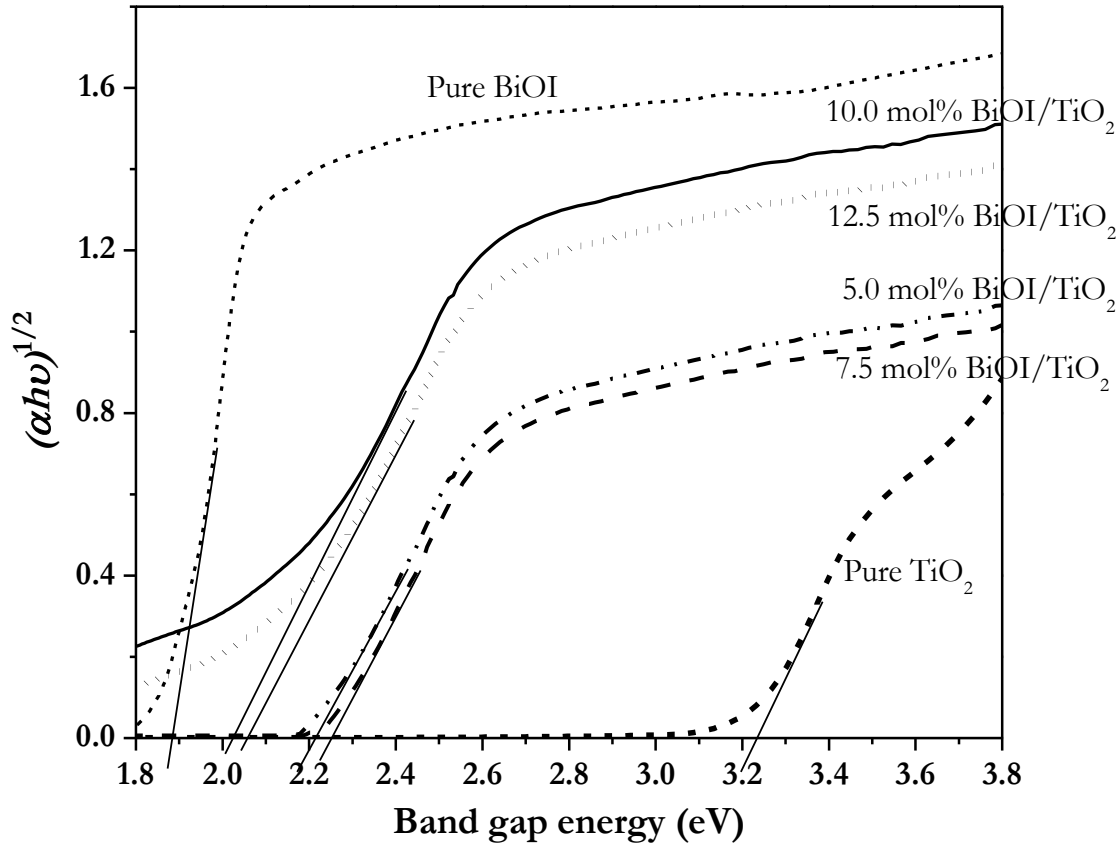


Fig. 4. (a) KM absorption spectra and (b) band gap energy of different Bi/Ti mole ratios.

### 3.3. Photocatalytic Activities and PL Properties of the Photocatalyst

The performance of phenol degradation over the entire catalysts is shown in Fig. 5. The photocatalytic activity in case of Degussa P25 is only 5.7%; whereas pure  $\text{TiO}_2$  and pure BiOI synthesized in this work exhibit slightly higher efficiencies of 9.1% and 8.4%, respectively. However, all BiOI/ $\text{TiO}_2$  nanocomposite photocatalysts show remarkably better degradation performance than pure  $\text{TiO}_2$ , pure BiOI and Degussa P25. A drastic reduction of electron-hole recombination rate as observed from PL analysis (Fig. 6) also confirms an excellent electron-hole separation efficiency of the composite materials, hence enhanced photocatalytic performance can be acquired in this work [24]. Additionally, simultaneous agglomeration of  $\text{TiO}_2$  and BiOI and the close interfacial connection between BiOI and  $\text{TiO}_2$  in the composite material as clearly observed from SEM and TEM results also suggest a better electron-hole transfer. Thus, more electrons would be available for the generation of  $\cdot\text{OH}$  radical [25], resulting in the enhancement of the photocatalytic performance as observed in this study. The results clearly show that the phenol degradation activity is improved as the BiOI amount in the composite increases. However, further increasing the BiOI to 12.5 mol% instead leads to a decrease of photocatalytic efficiency. This is probably due to its lower  $S_{\text{BET}}$  compared to the 10 mol% as evidenced from BET results in Table 1.

In order to explain the kinetic rate constant, a plot between  $-\ln(C_t/C_0)$  versus irradiation time (Fig. 7) was performed according to Eq. (3) [26]:

$$-\ln(C_t/C_0) = kK_t \quad (3)$$

where  $k$  is the true rate constant and  $K_t$  is the Langmuir adsorption equilibrium constant. Pseudo-first order degradation rate constants ( $k$ ) and correlation coefficient ( $R^2$ ) of photocatalytic degradation of phenol over all synthesized photocatalysts are shown in Fig. 7 and Table 2. The high correlation coefficient obtained in this work suggests that the phenol photodegradation over BiOI/ $\text{TiO}_2$  nanocomposite follows

pseudo-first order kinetic and the highest rate constant of  $3.7 \times 10^{-3} \text{ min}^{-1}$  is obtained from 10.0 mol% BiOI/TiO<sub>2</sub>, the best catalyst in this work.

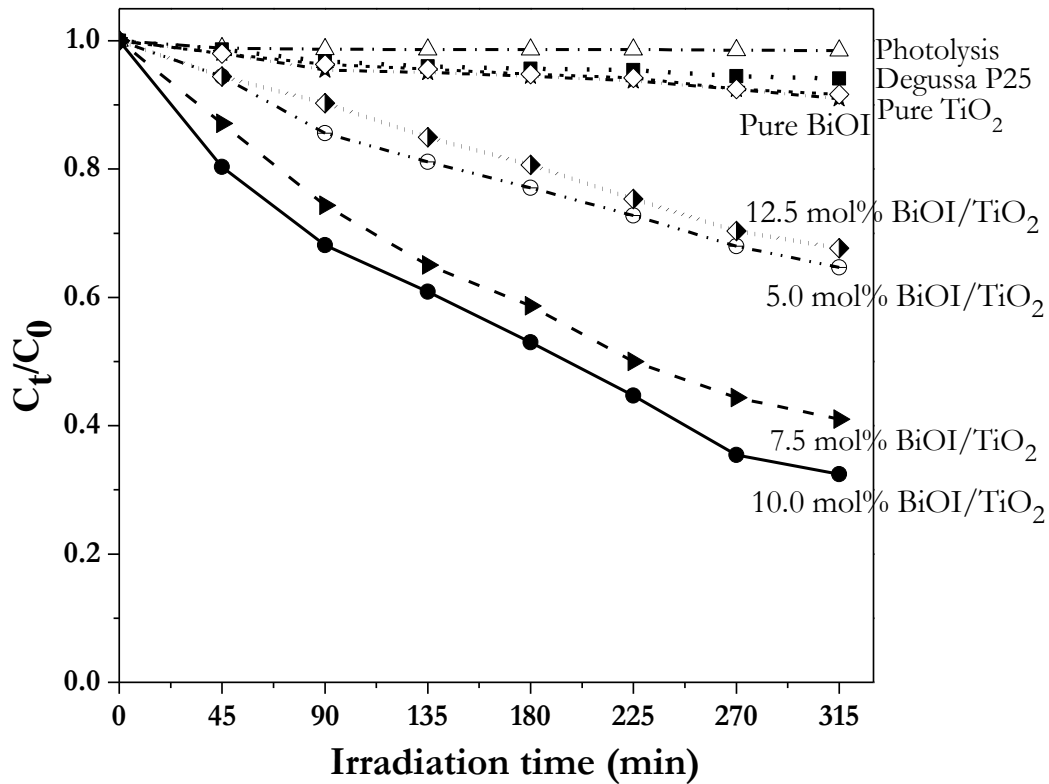


Fig. 5. Phenol photodegradation efficiencies over synthesized catalysts.

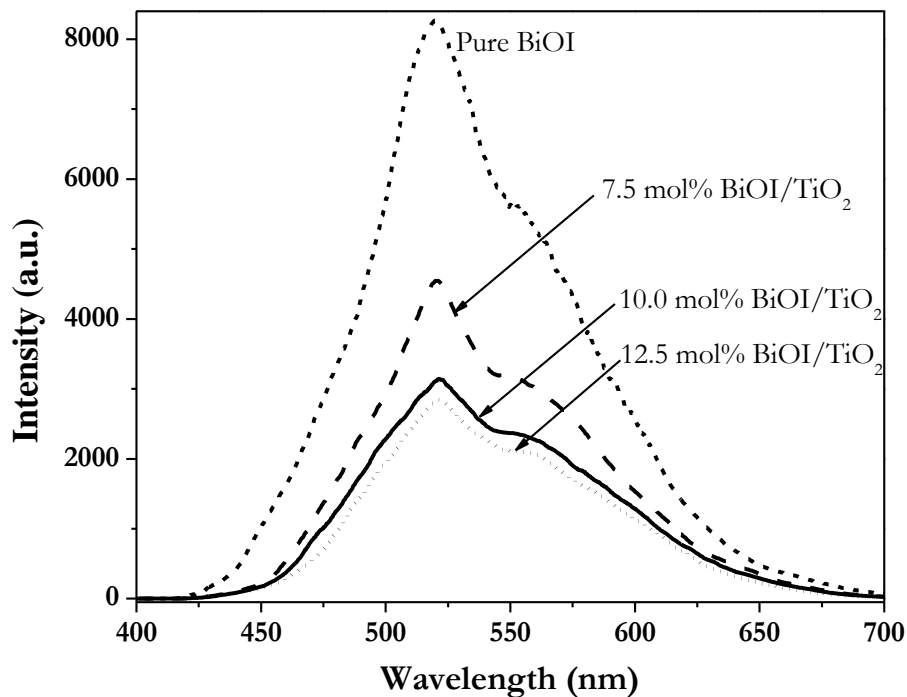


Fig. 6. Photoluminescence (PL) spectra of pure BiOI, 7.5 mol% BiOI/TiO<sub>2</sub>; 10.0 mol% BiOI/TiO<sub>2</sub> and 12.5 mol% BiOI/TiO<sub>2</sub>, respectively.

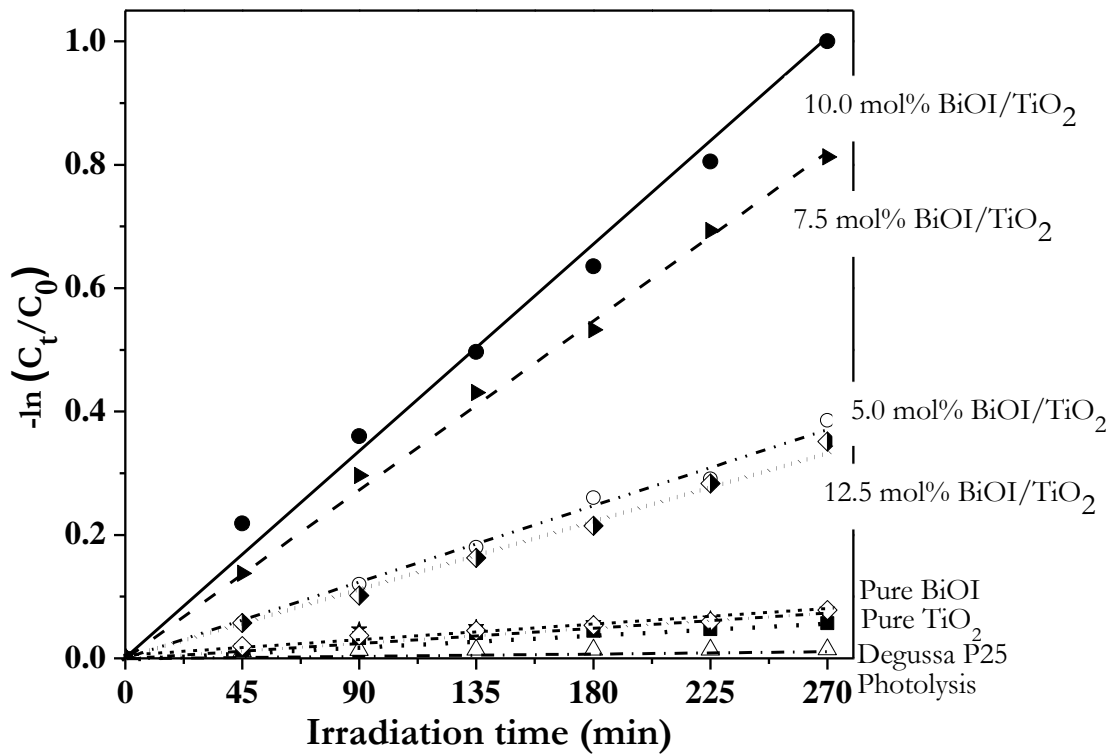


Fig. 7. Pseudo-first order degradation rate of photocatalytic degradation of phenol over the catalysts.

Table 2. Pseudo-first order degradation rate constants ( $k$ ) and correlation coefficient ( $R^2$ ) of photocatalytic degradation of phenol over all synthesized photocatalysts.

Sample	$k$ ( $\text{min}^{-1}$ )	$R^2$
Direct photolysis	$7.0 \times 10^{-5}$	0.9908
Pure $\text{TiO}_2$	$3.1 \times 10^{-4}$	0.9942
Pure BiOI	$3.3 \times 10^{-4}$	0.9904
5.0 mol% BiOI/ $\text{TiO}_2$	$1.4 \times 10^{-3}$	0.9930
7.5 mol% BiOI/ $\text{TiO}_2$	$3.1 \times 10^{-3}$	0.9975
10.0 mol% BiOI/ $\text{TiO}_2$	$3.7 \times 10^{-3}$	0.9901
12.5 mol% BiOI/ $\text{TiO}_2$	$1.3 \times 10^{-3}$	0.9953

#### 4. Conclusions

The BiOI/ $\text{TiO}_2$  nanocomposites are successfully synthesized by a two-step co precipitation/solvothermal method. XRD patterns exhibit characterization peaks of both BiOI and anatase  $\text{TiO}_2$  phase. The nanocomposites have the average particle size in the range of 15–30 nm. Phenol degradation performance of the prepared composites is investigated under visible light irradiation. The maximum phenol degradation of 68% with the highest pseudo-first order degradation rate is found in the case of 10.0 mol% BiOI/ $\text{TiO}_2$ . The enhanced catalytic performance observed from the BiOI/ $\text{TiO}_2$  composite might be ascribed to the significant reduction of band gap energy from 3.22 eV of pure  $\text{TiO}_2$  to 2.04 eV of the 10.0 mol% BiOI/ $\text{TiO}_2$  sample. A drastic reduction of electron-hole recombination rate from PL analysis also suggests an excellent electron-hole separation efficiency of this material, hence enhanced photocatalytic performance can be achieved in this work.

## Acknowledgements

This research was financially supported by the Uttaradit Rajabhat University, Uttaradit, Thailand, the Department of Chemistry, Department of Biology and Science & Technology Center, Faculty of Science and Technology. In this time, Dr. Boonprakob would like to thank Dr. Daungdao Channei and Mr. Paruchai Pongwan for SEM and TEM samples preparation.

## References

- [1] C. Chiou and R. Juang, "Photocatalytic degradation of phenol in aqueous solutions by Pr-doped TiO<sub>2</sub> nanoparticles," *Journal of Hazardous Materials*, vol. 149, no. 1, pp. 1–7, Oct. 2007.
- [2] S. Ahmed, M. Rasul, N. Wayde, N. Martens, R. Brown, and M. Hashi, "Heterogeneous photocatalytic degradation of phenols in wastewater: A review on current status and development," *Desalination*, vol. 261, no.1–2, pp. 3–18, Oct. 2010.
- [3] C. McManamon, J. Holmes, and M. Morris, "Improved photocatalytic degradation rates of phenol achieved using novel porous ZrO<sub>2</sub>-doped TiO<sub>2</sub> nanoparticulate powders," *Journal of Hazardous Materials*, vol. 193, no. 7, pp. 120–127, Oct. 2011.
- [4] S. Pardeshi and A. Patil, "A simple route for photocatalytic degradation of phenol in aqueous zinc oxide suspension using solar energy," *Solar Energy*, vol. 82, no. 8, pp. 700–705, Aug. 2008.
- [5] L. Wang, Z. Nie, C. Cao, M. Ji, L. Zhou, and X. Feng, "Controllable synthesis of porous TiO<sub>2</sub> with a hierarchical nanostructure for efficient photocatalytic hydrogen evolution," *Journal of Materials Chemistry A*, vol. 3, no. 1, pp. 3710–3718, Sep. 2014.
- [6] Z. Fan, F. Meng, J. Gong, H. Li, Y. Hu, and D. Liu, "Enhanced photocatalytic activity of hierarchical flower-like CeO<sub>2</sub>/TiO<sub>2</sub> heterostructures," *Materials Letters*, vol. 175, no. 4, pp. 36–39, Jul. 2016
- [7] T. Li, G. Chen, C. Zhou, Z. Shen, R. Jin, and J. Sun, "New photocatalyst BiOCl/BiOI composites with highly enhanced visible light photocatalytic performances," *Dalton Transactions*, vol. 40, no. 25, pp. 6751–6758, Dec. 2011.
- [8] M. Li, X. Li, G. Jiang, and G. He, "Hierarchically macro–mesoporous ZrO<sub>2</sub>–TiO<sub>2</sub> composites with enhanced photocatalytic activity," *Ceramics International*, vol. 41, no. 4, pp. 5749–5757, May 2015.
- [9] L. Zhang, G. Tan, S. Wei, H. Ren, A. Xia, and Y. Luo, "Microwave hydrothermal synthesis and photocatalytic properties of TiO<sub>2</sub>/BiVO<sub>4</sub> composite photocatalysts," *Ceramics International*, vol. 39, no. 8, pp. 8597–8604, Dec. 2013.
- [10] C. Chang, L. Zhu, Y. Fu, and X. Chu, "Highly active Bi/BiOI composite synthesized by one-step reaction and its capacity to degrade bisphenol A under simulated solar light irradiation," *Chemical Engineering Journal*, vol. 233, no. 1, pp. 305–314, Nov. 2013.
- [11] Z. Liu, X. Xu, J. Fang, X. Zhu, J. Chu, and B. Li, "Microemulsion synthesis, characterization of bismuth oxyiodine/titanium dioxide hybrid nanoparticles with outstanding photocatalytic performance under visible light irradiation," *Applied Surface Science*, vol. 258, no. 8, pp. 3771–3778, Feb. 2012.
- [12] Y. Li, J. Wang, B. Liu, H. Yao, and Z. Li, "BiOI-sensitized TiO<sub>2</sub> in phenol degradation: A novel efficient semiconductor sensitizer," *Chemical Physics Letters*, vol. 508, no.1–3, pp.102–106, May 2011.
- [13] Y. Chen, X. Xu, J. Fang, G. Zhou, Z. Liu, S. Wu, W. Xu, J. Chu, and X. Zhu, "Synthesis of BiOI-TiO<sub>2</sub> composite nanoparticles by microemulsion method and study on their photocatalytic activities," *Science World Journal*, vol. 2014, pp. 1–8, Jan. 2014.
- [14] C. Liao, Z. Guoping, and D. Li, "BiOI nanosheets decorated TiO<sub>2</sub> nanofiber: Tailoring water purification performance of photocatalyst in structural and photo-responsivity aspects," *Applied Surface Science*, vol. 314, no. 4, pp. 481–489, Sep. 2014.
- [15] N. Boonprakob, N. Wetchakun, S. Phanichphant, D. Waxler, P. Sherrell, A. Nattestad, J. Chen, and B. Inceesungvorn, "Enhanced visible-light photocatalytic activity of g-C<sub>3</sub>N<sub>4</sub>/TiO<sub>2</sub> films," *Journal of Colloid and Interface Science*, no. 1, vol. 417, pp. 402–409, Dec. 2014.
- [16] P. Jansanthea, N. Boonprakob, J. Treenattip, P. Pookmanee, and S. Phanichphant, "Photocatalytic degradation of methylene blue and methyl orange over TiO<sub>2</sub> powder synthesized via the solvothermal method," *Applied Mechanics and Materials*, vol. 749, no. 1, pp. 51–55, Jan. 2015.

- [17] L. Huiquan, C. Yumina, H. Wenshan, H. Lin, and T. Dongliang, "Studies on synergistic solvent extraction of rare earth elements from nitrate medium by mixtures of 8-hydroxyquinoline with Cyanex 301 or Cyanex 302," *Rare Metals*, vol. 3, no. 6, pp. 604–608, Jun. 2013.
- [18] A. Burton, K. Ong, T. Rea, P. Ignatius, and Y. Chan, "On the estimation of average crystallite size of zeolites from the Scherrer equation: A critical evaluation of its application to zeolites with one-dimensional pore systems," *Microporous and Mesoporous Materials*, vol. 117, no.1–2, pp. 75–90, Jan. 2009.
- [19] W. Kim, T. Tachikawa, H. Kim, N. Lakshminarasimhan, P. Murugan, H. Park, T. Majima and W. Choi, "Visible light photocatalytic activities of nitrogen and platinum-doped TiO<sub>2</sub>: Synergistic effects of co-dopants," *Applied Catalysis B: Environmental*, vol. 147, no. 1, pp. 642–650, Apr. 2014.
- [20] M. Suwarnkar, R. Dhabbe, A. Kadam, and K. Garadkar, "Enhanced photocatalytic activity of Ag doped TiO<sub>2</sub> nanoparticles synthesized by a microwave assisted method," *Ceramics International*, vol. 40, no. 4, pp. 5489–5496, May 2014.
- [21] S. Wang, L. Wang, W. Ma, D. Johnson, Y. Fang, M. Jia, and Y. Huang, "Moderate valence band of bismuth oxyhalides (BiOXs, X = Cl, Br, I) for the best photocatalytic degradation efficiency of MC-LR," *Chemical Engineering Journal*, vol. 259, no. 1, pp. 410–416, Jan. 2015.
- [22] P. Pongwan, B. Inceesungvorn, K. Wetchakun, S. Phanichphant, and N. Wetchakun, "Highly efficient visible-light-Induced photocatalytic activity of Fe-doped TiO<sub>2</sub> nanoparticles," *Engineering Journal*, vol. 16, no. 3, pp. 143–151, Jul. 2011.
- [23] T. Li, G. Chen, Z. Shen, and R. Jin, "New photocatalyst BiOCl/BiOI composites with highly enhanced visible light photocatalytic performances," *Dalton Transactions*, vol. 40, no. 25, pp. 6751–6758, May 2011.
- [24] N. Boonprakob, N. Wetchakun, S. Phanichphant, J. Chen, and B. Inceesungvorn, "N-loaded TiO<sub>2</sub> for photocatalytic degradation of methyl orange under visible light irradiation," *Advanced Materials Research Journal*, vol. 622, pp. 883–888, Oct. 2013.
- [25] J. Jiang, X. Zhang, P. Sun, and L. Zhang, "ZnO/BiOI Heterostructures: Photoinduced charge-transfer property and enhanced visible-light photocatalytic activity," *The Journal of Physical Chemistry C*, vol. 115, no. 42, pp. 20555–20564, Sep. 2011.
- [26] N. Kumar, A. Couzis, and C. Maldarelli, "Measurement of the kinetic rate constants for the adsorption of superspreading trisiloxanes to an air/aqueous interface and the relevance of these measurements to the mechanism of superspreading," *Journal of Colloid and Interface Science*, vol. 267, no. 2, pp. 272–285, Nov. 2003.